Kobe University Repository : Kernel

PDF issue: 2025-12-05

Annealing process for recovery of carbonated (Mg,Ca)O protective layer for plasma discharge device

Takeda, Eiji
Zukawa, Takehiro
Tsujita, Takuji
Yoshino, Kyohei
Morita, Yukihiro

(Citation)
Japanese Journal of Applied Physics,57(9):096001

(Issue Date)
2018-08-03

(Resource Type)
journal article

(Version)
Accepted Manuscript

(Rights)
© 2018 The Japan Society of Applied Physics. This is the Accepted Manuscript version of an article accepted for publication in Japanese Journal of Applied Physics. IOP Publishing Ltd is not responsible for any errors or omissions in this version of the manuscript or any version derived from it. The Version of Record is available online…

(URL)
https://hdl.handle.net/20.500.14094/90008074

Annealing process for recovery of carbonated (Mg,Ca)O protective layer for plasma discharge device

Eiji Takeda[1,2]*, Takehiro Zukawa[3], Takuji Tsujita[4], Kyohei Yoshino[5], and Yukihiro Morita[3,6]

[1] *Department of Electric and Electronic Engineering, Graduate School of Engineering, Kobe University, Kobe 657-8501, Japan*
[2] *Sensing Solution Development Center, Engineering Division, Automotive & Industrial Systems Company, Panasonic Corporation, Kadoma, Osaka 571-8506, Japan*
[3] *Institute for Sensors and Devices, Technology Innovation Division, Panasonic Corporation, Kadoma, Osaka 571-8508, Japan*
[4] *Institute for Energy and Material / Food Resources, Technology Innovation Division, Panasonic Corporation, Kadoma, Osaka 571-8508, Japan*
[5] *Automotive Infotainment Systems Business Division, Automotive & Industrial Systems Company, Panasonic Corporation, Yokohama 224-8520, Japan*
[6] *Panasonic Device Science Research Alliance Laboratory, Graduate School of Engineering, Osaka University, Suita, Osaka 565-0871, Japan*

The carbonation behavior and decarbonation annealing of a protective (Mg,Ca)O layer for flat panel plasma discharge devices were investigated. Compared with a conventional MgO protective layer, the (Mg,Ca)O protective layer showed both high and low discharge voltages. Quantitative X-ray photoelectron spectroscopy analyses indicated that the high discharge voltages were caused by Ca carbonation. The progression of Ca carbonation was enhanced by exposure to air containing H_2O but not by exposure to dry air. In addition, once (Mg,Ca)O is carbonated, it is impossible to decarbonate Ca by annealing in air at the temperature applied during the production process. We propose the use of annealing in vacuum as an effective method to promote the decarbonation of Ca and maintain a low discharge voltage for plasma discharge devices with (Mg,Ca)O protective layers.

1. Introduction

It is well known that dielectric barrier discharge is an effective and efficient technology to generate plasmas.[1)] In particular, Xe plasma has attracted much attention as a mercury-free ultraviolet source, and it is applied to not only cylindrical fluorescent lamps but also flat panel plasma discharge devices such as plasma displays,[2–4)] planar lighting,[5,6)] and plate-type virus inactivation devices.[7,8)] In these plasma discharge devices, a Ne:Xe mixed gas is often used

*E-mail: takeda.eiji@jp.panasonic.com

as the discharge gas to reduce the discharge voltage by the Penning effect, and visible or deep ultraviolet light is emitted from the internal phosphors excited by vacuum ultraviolet (VUV) that the Xe plasma radiates. Electron emission from a dielectric cathode plays an important role in generating and sustaining a plasma. In addition, the dielectric barrier discharge voltage is strongly dependent on the ion-induced secondary electron emission coefficient (γ) at the surface of the dielectric cathode layer.[9] Therefore, a dielectric electron emitter with an appropriate γ coefficient is a key material for enhancing the dielectric barrier discharge properties in plasma discharge devices.

To protect the electrode and dielectric layer against sputtering by discharges, an oxide protective layer is formed at the surface of the dielectric layer in such plasma discharge devices. MgO is often used as the oxide protective layer because of its relatively high γ, chemical stability, and resistance to sputtering. A high Xe content in the Ne:Xe mixed discharge gas in plasma discharge devices is effective for enhancing the VUV generation efficiency; however, the discharge voltage also increases simultaneously in the case of a MgO protective layer because MgO has a low γ for Xe.[10–12] Therefore, materials with a higher γ than conventional MgO should have both high VUV generation efficiency and low discharge voltage for plasma discharge devices with a high Xe content.

As higher-γ materials, CaO, SrO, and (Sr,Ca)O were studied previously.[13–15] However, the practical application of these materials as protective layers has not been realized, because they largely adsorb H_2O and CO_2 in air owing to the enhanced reactivity at O^{2-} sites.[16,17] Many other materials have also been reported,[18–21] but their practical use has not been realized for similar reasons. To suppress the effects of chemical reactivity and obtain optimal performance of plasma discharge devices with these materials as protective layers, an all-in-vacuum process[22] or a structure with double protective layers[23,24] has been proposed, but these are difficult to practically apply in production.

The material with the highest potential as a higher-γ protective layer is (Mg,Ca)O.[25–30] (Mg,Ca)O is relatively stable compared with the other materials described above because it is MgO-based. Many groups report that low discharge voltages are obtained relative stably with a (Mg,Ca)O protective layer. However, extensive quantitative analyses of the relationship between discharge voltage and the chemical state of the (Mg,Ca)O protective layer have yet to be performed. Moreover, a suitable process to obtain the best performance of the (Mg,Ca)O protective layer for the production of plasma discharge devices has not yet been proposed.

In this study, we investigate the chemical factors related to discharge voltage when (Mg,Ca)O is used as a protective layer for plasma discharge devices. Plasma display pan-

Table I. Specifications of the test panels used in this study.

Front Panel	
ITO electrode width	110 μm
Bus electrode width	65 μm
Electrode gap	80 μm
Dielectric layer thickness	39 μm
Protective layer thickness	800 nm
Back Panel	
Address electrode width	65 μm
Dielectric layer thickness	10 μm
Barrier rib height	120 μm
Barrier rib width	40 μm
Phosphor thickness	12 μm
Pixel size	480 × 160 μm^2

els are employed to evaluate dielectric barrier discharge voltage. Analysis of the surface of the (Mg,Ca)O protective layer enables the quantitative assignment of the chemical states of the (Mg,Ca)O protective layer related to discharge voltage. The effects of the exposure environment after deposition on the progression of chemical reactions related to discharge voltage are also demonstrated. An annealing process applicable to recovering the (Mg,Ca)O protective layer with degraded discharge voltage is also investigated.

2. Experimental methods

To investigate the effects of a (Mg,Ca)O protective layer on the discharge voltage in plasma discharge devices, 42 in. alternating current plasma display panels with full high definition were produced. MgO and (Mg,Ca)O films were deposited as protective layers by electron beam evaporation on the dielectric layers of the front panels. During the deposition, the substrate temperature was kept at 350 °C, and O_2 gas was continuously supplied to the chamber at 20 sccm. The evaporation targets for (Mg,Ca)O were sintered mixtures of MgO and CaO. The thickness of the protective layers was 800 nm. The CaO concentration in the (Mg,Ca)O protective layer was approximately 12 mol%. MgO powders were dispersed on the protective layers to improve the statistical discharge delay.[31] The panels were sealed with N_2 gas supplied to the space between the front and back panels. The Xe content used in the discharge gas was 100%. The pressure of Xe discharge gas in the panels was set to 225 Torr. The specifications of the test panels used in this study are shown in Table I.

The panels were kept in dry air after the deposition of the MgO and (Mg,Ca)O films to

suppress H_2O adsorption on the samples. In addition, the panels were only dismantled in dry air and the samples were kept in sealed packages filled with N_2 gas until the measurements. The dew point of the dry air was controlled to approximately −40 °C. The exposure time to normal air containing H_2O from unsealing the packages to introducing the samples into the vacuum chamber of the measurement system was less than 15 s.

The chemical states of C, O, Mg, and Ca in (Mg,Ca)O were characterized by X-ray photoelectron spectroscopy (XPS; Ulvac Phi, PHI Quantera SXM). The samples were excited by a monochromatic X-ray source with an Al Kα line at 1486.7 eV. The spot of incident X-rays was 50 μm in diameter. The photoelectron signals from the samples were detected at a take-off angle of 45° using a concentric hemispherical analyzer with pass energies of 69 eV for C-, O-, and Mg-related photoelectrons and 140 eV for Ca-related photoelectrons. The surfaces of the samples were neutralized by a combination of electrons and an Ar^+ beam to suppress charging effects during XPS.[32] Software for XPS analysis (Ulvac Phi, MultiPak) was used to subtract background signals for all photoelectron spectra according to the Shirley background.[33] Binding energies for the spectra were corrected by shifting the binding energy of hydrocarbon-related peaks at the C 1s photoelectron line to 284.8 eV.[34] C-, O-, Mg-, and Ca-related photoelectron signal intensities were corrected by setting the relative sensitivity factors in the measured regions to 21.479, 50.3, 13.546, and 76.596, respectively.

3. Results and discussion

Discharge sustaining voltage (V_{sus}) and luminous efficiency were measured for panels with MgO and (Mg,Ca)O protective layers produced under various conditions. A high luminous efficiency of approximately 1.6 lm/W was obtained for both MgO and (Mg,Ca)O protective layers. This is attributed to the enhancement of VUV generation efficiency due to the setting of the Xe content in the discharge gas to 100%. V_{sus} with a conventional MgO protective layer was stable at approximately 250 V; however, the variation in V_{sus} was much larger for the (Mg,Ca)O protective layer than for the conventional MgO layer, despite having the same Ca concentration. There were also panels with a higher V_{sus}, while a lower V_{sus} was realized as expected; the difference between the minimum and maximum V_{sus} values was approximately 85 V.

To investigate the reason for the above-mentioned difference in V_{sus}, the panels with various V_{sus} values were dismantled and the surfaces of the (Mg,Ca)O protective layers were analyzed by XPS. One of the difficulties in the analysis of protective layer surfaces is the effects of the adsorption of impurity gas from the air during the dismantling of the panels until

Table II. Production conditions and V_{sus} for panel Nos. 1, 2, and 3.

Condition	Panel No. 1	Panel No. 2	Panel No. 3
CaO conc. (mol%)	12	12	12
Annealing atmosphere prior to panel sealing	Vacuum	Air	Air
Annealing atmosphere during panel sealing	N_2	N_2	Air
V_{sus} (V)	210	237	262

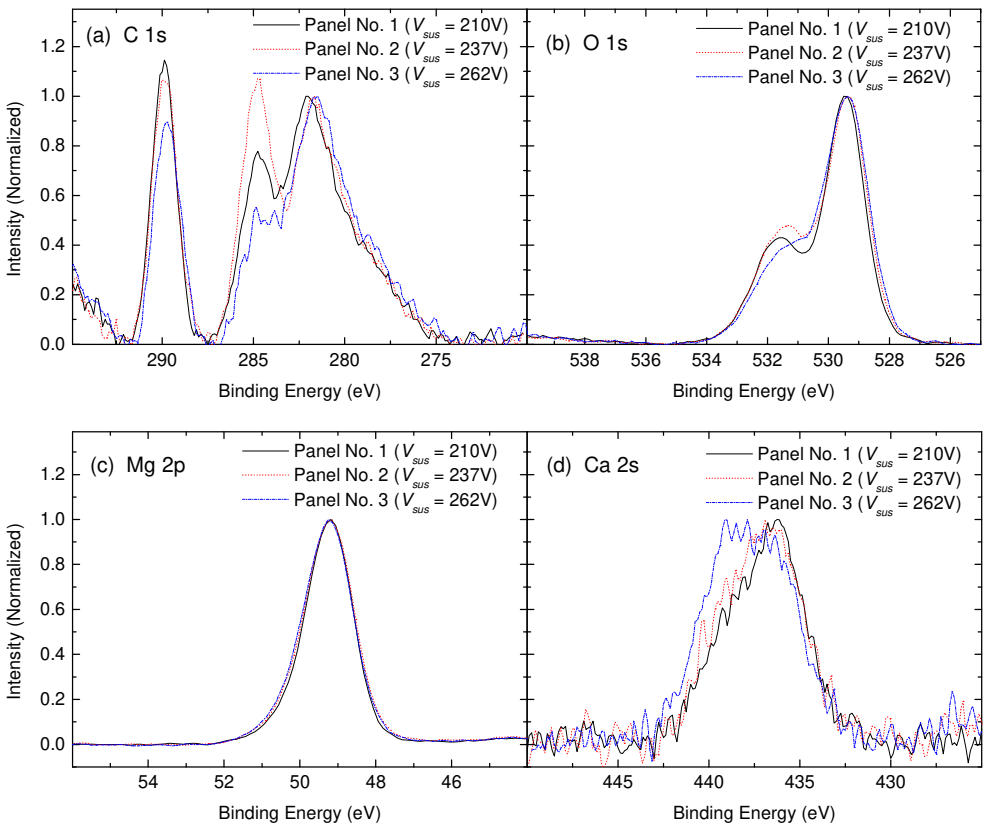

Fig. 1. (Color online) (a) C 1s, (b) O 1s, (c) Mg 2p, and (d) Ca 2s photoelectron spectra for (Mg,Ca)O protective layers from panel Nos. 1, 2, and 3 with V_{sus} values of 210, 237, and 262 V, respectively.

the samples are introduced into the measurement chamber. To suppress the adsorption of H_2O in particular, the samples were dismantled in dry air and stored in a N_2 atmosphere until the measurements. In addition, to take into account both chemical and physical adsorptions, not only Mg- and Ca-related photoelectron spectra were measured but also C- and O-related photoelectron spectra, and the relationship between V_{sus} and the adsorption states obtained from

each spectrum was investigated. The C 1s, O 1s, Mg 2p, and Ca 2s photoelectron spectra results for panel Nos. 1, 2, and 3 with respective V_{sus} values of 210, 237, and 262 V are shown in Figs. 1(a)-1(d), respectively. The production conditions of these panels are summarized in Table II. The C 1s and O 1s photoelectron spectra were measured to quantify the amounts of the C=O, C−H (or C−C), and O−H bonding states adsorbed on the (Mg,Ca)O protective layer. The chemical states of Mg and Ca were characterized by analyzing the Mg 2p and Ca 2s photoelectron spectra. Mg 2p photoelectrons provide one of the most intense lines for Mg, whereas Ca 2s photoelectrons do not provide such an intense line for Ca. The kinetic energy of Ca 2p photoelectrons, which show the most intense line for Ca, overlaps with that of Mg KLL Auger electrons when using the Al Kα line as an X-ray excitation source; therefore, the Ca 2s photoelectron line was analyzed instead. The spectra were normalized with respect to the peak values of Mg-related signals in Fig. 1(a) and each photoelectron peak in Figs. 1(b)-1(d).

Figure 1(a) shows three peaks obtained in C 1s photoelectron spectra. The peaks with binding energies of approximately 290 and 285 eV can be assigned to the C=O and C−H (or C−C) bonding states, respectively.[35,36] Mg-related Auger electron lines appear as a broad peak at approximately 282 eV in the case of Al Kα X-ray excitation.[37] The O 1s photoelectron spectra in Fig. 1(b) have peaks with shoulders on the high-binding-energy side. The bonding states of O atoms at binding energies of approximately 529, 531, and 532 eV are assigned to Mg or Ca oxidation, and the O−H and C=O bonding states, respectively.[36,38] The Mg 2p photoelectron spectra shown in Fig. 1(c) have a chemical state assigned to Mg oxidation at a binding energy of 49 eV,[36] which remains almost unchanged, despite the change in V_{sus}. On the other hand, the Ca 2s photoelectron spectra shift to higher binding energies with increasing V_{sus}, as shown in Fig. 1(d). It is assumed that this shift to a higher binding energy of approximately 439 eV in the Ca 2s photoelectron spectra is related to the carbonation state of Ca[38,39] owing to the relatively higher chemisorption nature of CO_2 toward Ca.[40,41] The lower binding energy of the Ca 2s photoelectron line at approximately 436 eV is attributed to the oxidation state of Ca.[38]

By fitting the spectra in Figs. 1(a) and 1(b) with Gaussian functions, the amounts of the C=O, C−H (or C−C), and O−H bonding states adsorbed on the (Mg,Ca)O protective layers can be calculated. Although the amount of the C=O bonding state can be obtained from both C 1s and O 1s photoelectron spectra, it was calculated from the C 1s spectra. The ratio of Ca carbonation $[G_c/(G_o + G_c)]$ can also be estimated by fitting the Ca 2s photoelectron spectra with two Gaussian functions for the oxidation (G_o) and carbonation states (G_c). Figures 2(a)-

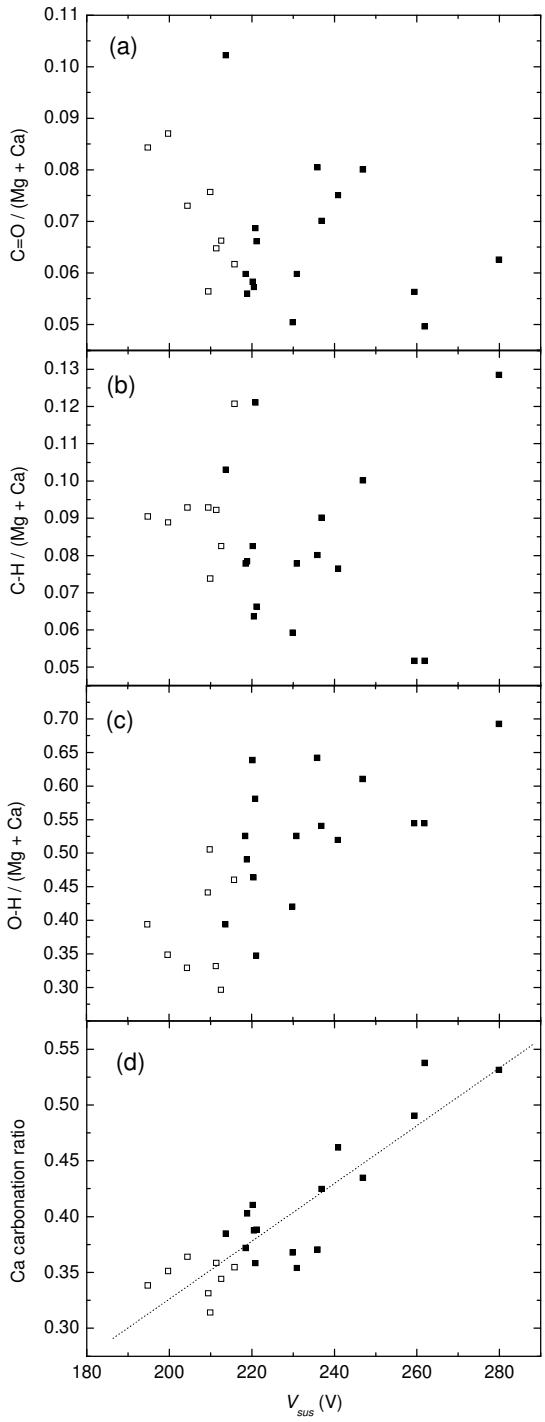

Fig. 2. Relationship between V_{sus} and the amounts of the (a) C=O, (b) C−H and (c) O−H bonding states, and (d) the Ca carbonation ratio $G_{\mathrm{c}}/(G_{\mathrm{o}} + G_{\mathrm{c}})$ on (Mg,Ca)O protective layers. Squares correspond to experimentally obtained data, while the dotted line shows a linear fit. Open symbols correspond to data from the panels annealed in vacuum, while closed symbols to data obtained under other annealing conditions.

2(c) show the relationship between V_{sus} and the amounts of the C=O, C−H, and O−H bonding states adsorbed on the (Mg,Ca)O protective layer, respectively. These amounts are normalized according to the sum of the Mg and Ca signals, because the absolute values of the spectra can be verified among the samples from the charging effects. The relationship between V_{sus} and the Ca carbonation ratio $G_c/(G_o + G_c)$ is also shown in Fig. 2(d), where the dotted line is a linear fit. The relationship between V_{sus} and the amounts of the C=O, C−H and O−H bonding states is very poor, while V_{sus} well correlates with the Ca carbonation ratio. Figure 2(d) shows that, as the Ca carbonation is enhanced, V_{sus} increases. The analysis of the depth profiles of photoelectron signals from carbon has revealed that the depth of the presence of carbon from the surface is related to the discharge voltage for a (Ca,Mg)O protective layer with different CaO concentrations.[42] We have directly demonstrated that no carbonation of the (Mg,Ca)O protective layer in the panels occurs at Mg sites, but that it occurs predominantly at Ca sites; the carbonation ratio is clearly related to discharge voltage, even at the same CaO concentration.

A contradiction between Figs. 2(a) and 2(d) is evident; the correlations show disagreement even if the vertical axes in both Figs. 2(a) and 2(d) indicate the C=O bonding state or carbonation. The reason for this is thought to be as follows. The changes in the Ca 2s photoelectron spectra are caused only by chemical adsorption, because the Ca bonding state is modified only by chemical reactions. In contrast, the C 1s photoelectron signals indicate both physical and chemical adsorptions, and it is difficult to separate the spectra from each other. The amount of adsorption varies with exposure time in air from the dismantling of the panels until the measurements are performed, especially in the case of immediate physical adsorption. Therefore, the amounts of C=O bonding states that are not originally present in the panels may be detected largely in C 1s photoelectron spectra. The poor correlation in Figs. 2(b) and 2(c) can also be explained similarly. Therefore, we consider that Ca 2s photoelectron spectra are more suitable for the quantification of the amount of adsorption in the panels because chemical adsorption proceeds more slowly than physical adsorption.

Considering the results shown in Fig. 2(d), the good correlation between V_{sus} and the amount of carbonated (Mg,Ca)O can be explained by electron emission with Auger neutralization.[43,44] Figure 3 shows a schematic energy diagram of the electron emission processes from bulk MgO by Auger neutralization for Ne^+ and Xe^+. In these processes, a wider band gap indicates a lower γ if the electron affinity is equivalent. The wide band gap for bulk MgO indicates that electron emission is effective via Ne^+, but not via Xe^+. However, the band gap at the surface in a thin film is reduced owing to crystal structure imperfections, which gener-

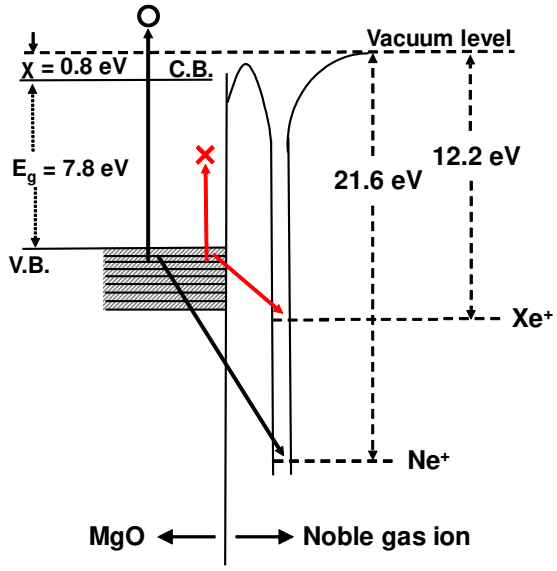

Fig. 3. (Color online) Schematic energy diagram for electron emission processes from bulk MgO by Auger neutralization via Ne^+ and Xe^+.

ate extra states in the band gap. Therefore, electron emission from the surface states of MgO can be slightly effective, even for Xe^+. The band gaps of MgO, $MgCO_3$, CaO, and $CaCO_3$ were estimated by computational simulations of the density of states using the WIEN2k program.[45] Although these values are somewhat different from the actual values because of the limits of the band theory calculations, the relative changes in band gaps from the oxidation states to the carbonation states for Mg and Ca can be discussed. The relative band gaps of MgO:CaO, MgO:$MgCO_3$, and CaO:$CaCO_3$ were determined to be 1:0.77, 1:1.04, and 1:1.38, respectively. A comparison of MgO with CaO indicates that the higher γ for CaO is explained by its narrower band gap. The degradation of γ is noticeable owing to the formation of a much wider band gap by the carbonation of CaO than by that of MgO. Consequently, it is suggested that the band gap is narrower for (Mg,Ca)O than for MgO, which leads to a higher γ, but the band gap is significantly increased by carbonation, which results in a lower γ and a higher V_{sus}.

To understand the progression of the chemical carbonation of Mg and Ca in various atmospheres, (Mg,Ca)O films were exposed to N_2, dry air, and normal air atmospheres for 14 days immediately after deposition, and the surfaces were then analyzed by XPS. The Mg 2p and Ca 2s photoelectron spectra are shown in Figs. 4(a) and 4(b), respectively. The spectra are also normalized with respect to the peak values. The $G_c/(G_o + G_c)$ ratios obtained from Fig. 4(b) are shown in Table III. The Mg 2p photoelectron peaks show that the carbonation of Mg

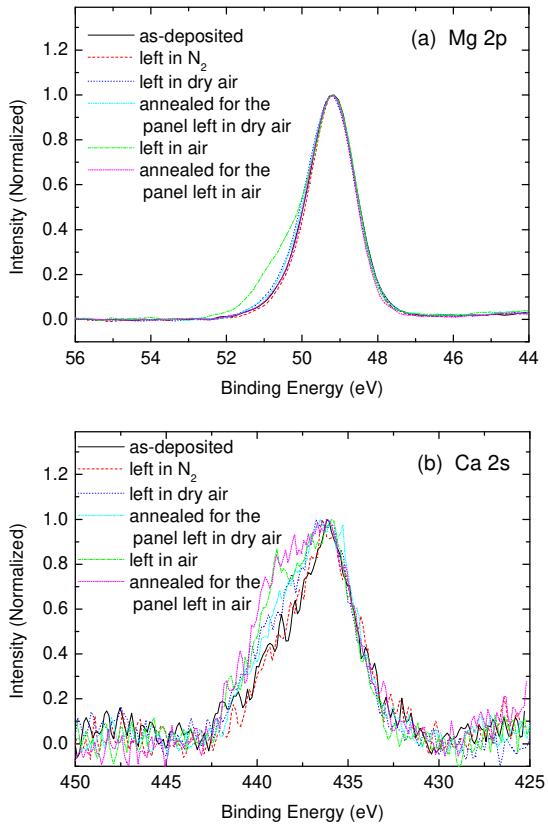

Fig. 4. (Color online) (a) Mg 2p and (b) Ca 2s photoelectron spectra of (Mg,Ca)O films after exposure to N_2, dry air, and normal air atmospheres for 14 days after deposition. Spectra of the as-deposited sample and the samples annealed in air at 350 °C after exposure to dry air and air atmospheres are also shown.

Table III. Ca carbonation ratios $[G_c/(G_o + G_c)]$ obtained from Fig. 4(b).

Condition	G_c / (G_o + G_c)
As-deposited	0.29
Left in N_2	0.3
Left in dry air	0.35
Annealed for the panel left in dry air	0.37
Left in air	0.45
Annealed for the panel left in air	0.49

proceeds only in the air atmosphere.[46] This carbonation can be reversed by annealing in air at 350 °C. The possible reason why the V_{sus} of a conventional panel with a MgO protective

layer is stable is the reversal from the carbonation to oxidation of Mg by annealing in air, even if the carbonation of Mg proceeds.

On the other hand, the Ca 2s photoelectron peaks indicate that the chemical state of Ca remains unchanged only in the N_2 atmosphere. Although Ca carbonation proceeds readily in normal air, the carbonation is suppressed to some extent in dry air. Therefore, we suggest that H_2O in air enhances Ca carbonation because it has been reported that moisture is often added to the CaO carbonation process to increase the reaction rate owing to the formation of the $Ca(OH)_2$ intermediate.[47] In addition, the carbonation of Ca is not reversed by oxidation owing to annealing in air at 350 °C, but is enhanced slightly. Extreme ultraviolet photoelectron spectroscopy (EUPS) measurements of MgO and CaO showed that the amount of CO_2 adsorbed was increased by annealing in air for CaO, but not for MgO.[48] Metastable de-excitation spectroscopy (MDS) measurements showed that the ionization potential was almost unchanged for MgO, but significantly increased for CaO by annealing in air.[49] The results of the annealing of (Mg,Ca)O thin films in air in this study are similar to those of MgO and CaO films measured by EUPS and MDS. We suggest that the reversal of Ca carbonation by annealing in air is impossible, which is the reason why the V_{sus} of panels with a (Mg,Ca)O protective layer is unstable because there are differences in the degree of Ca carbonation under various production conditions and exposure time in the atmosphere after (Mg,Ca)O deposition. This is considered to be critical for (Mg,Ca)O protective layers because detailed control of exposure time in the atmosphere after deposition, i.e., the degree of Ca carbonation, is difficult during the production.

It is thus necessary to introduce a process to overcome this problem to the production of the (Mg,Ca)O protective layer to suppress carbonation. We investigated the decarbonation and carbonation behaviors of air-annealed (Mg,Ca)O films using various additional annealing procedures in N_2, vacuum, N_2:H_2O, N_2:CH_4, and N_2:CO_2 atmospheres at 500 °C. The pressure for vacuum annealing was in the range from 10^{-5} to 10^{-4} Torr. N_2 and the mixture gases were continuously supplied during annealing at 10 L/min. The N_2:H_2O gas flow was realized by bubbling pure water with N_2 gas. Figures 5(a) and 5(b) show the Mg 2p and Ca 2s photoelectron spectra of the (Mg,Ca)O films with the additional annealing after annealing in air, respectively; thus, the spectrum for annealing in air indicates the initial chemical state of this trial. The $G_c/(G_o + G_c)$ ratios obtained from Fig. 5(b) are shown in Table IV. For both Mg and Ca, the photoelectron spectral shift to higher binding energies was more significant after annealing in the N_2:CO_2 atmosphere. Relatively large shifts to higher binding energies resulted from annealing in the N_2:CH_4 and N_2:H_2O atmospheres for Ca than for Mg. The

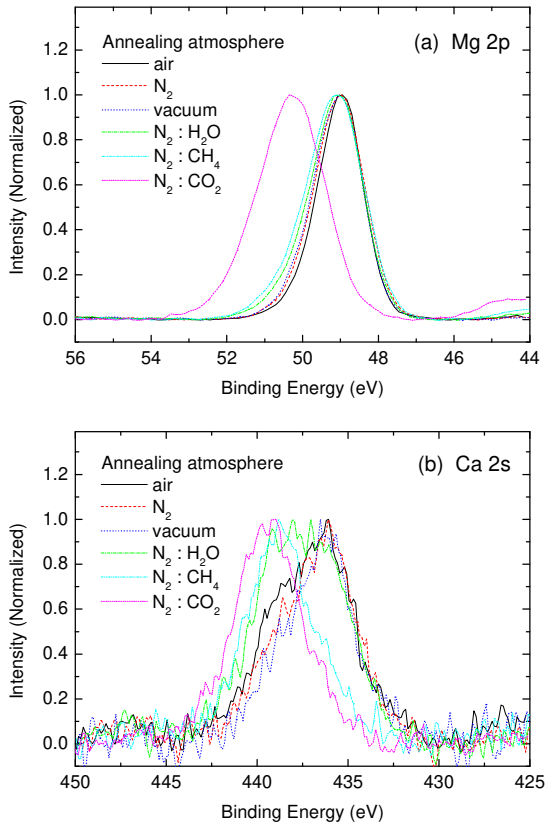

Fig. 5. (Color online) (a) Mg 2p and (b) Ca 2s photoelectron spectra of (Mg,Ca)O films with the additional annealing in N_2, vacuum, N_2:H_2O, N_2:CH_4, and N_2:CO_2 atmospheres after annealing in air. The spectrum for annealing in air indicates the initial chemical state of this trial. The annealing temperatures were 350 °C in air and 500 °C in the other atmospheres.

spectral changes induced by annealing in the N_2:CO_2 atmosphere are due to the carbonation of Mg and Ca.[38,39,46] The chemical states of Ca can also be changed, even in the N_2:CH_4 and N_2:H_2O atmospheres. It has been reported that the ionization potential of CaO can be changed by the adsorption of H_2O or CO_2, as confirmed by MDS measurements.[50] The degree of change in the ionization potential by H_2O or CO_2 adsorption is similar to that of the spectral changes after annealing in N_2:CO_2 and N_2:H_2O gases. This suggests that the change in the chemical bonding states of Ca by H_2O or CO_2 chemisorption leads to an increase in ionization potential. Similarly, it is considered that the ionization potential is increased by the changes in the chemical bonding states of Ca due to CH_4 chemisorption. These results indicate that not only CO_2 gas but also moisture and organic compound gases remaining in the annealing atmosphere should be removed as much as possible to suppress an increase in ionization potential and the degradation of γ of the (Mg,Ca)O protective layer.

Table IV. Ca carbonation ratios $[G_c/(G_o + G_c)]$ obtained from Fig. 5(b).

Annealing atmosphere	$G_c / (G_o + G_c)$
Air	0.43
N_2	0.35
Vacuum	0.29
N_2:H_2O	0.57
N_2:CH_4	0.86
N_2:CO_2	0.97

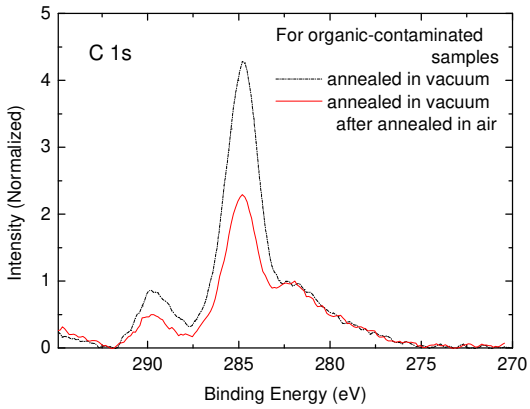

Fig. 6. (Color online) C 1s photoelectron spectra of (Mg,Ca)O films annealed in vacuum and air and vacuum combination after immersion in a solution of α-terpineol. The annealing temperatures were 350 °C in air and 500 °C in vacuum.

On the other hand, carbonation can be reversed by annealing in both N_2 atmosphere and vacuum. Annealing in vacuum was the most effective process for the decarbonation of the (Mg,Ca)O films, because the activation energy for the decarbonation of $CaCO_3$ is modified and the actual pressure of the thermally desorbed CO_2 is greatly reduced to less than the equilibrium pressure between the carbonation and decarbonation reactions especially in vacuum.[51] In Fig. 2(d), data from panels with a (Mg,Ca)O protective layer that were annealed in vacuum are also plotted with open symbols. These data are obtained at V_{sus} values from 195 to 215 V with a low carbonation ratio of the (Mg,Ca)O protective layer. Although V_{sus} was also changed by the species adsorbed on the front or back panel and by the process conditions for panel sealing,[30] it is demonstrated that annealing of a carbonated (Mg,Ca)O protective layer in vacuum is effective for reducing V_{sus} owing to the decarbonation of Ca.

In the conventional production processes for plasma discharge devices, organic residues can be removed by annealing the panel in air. As described above, organic residues should be removed because the chemical states and γ at the (Mg,Ca)O surface are modified by the organic compounds desorbed during the panel sealing process at high temperatures. However, annealing in vacuum is considered to be ineffective for removing organic residues owing to a lack of O_2. In Fig. 6, C 1s photoelectron spectra are shown for the samples annealed in vacuum and air and vacuum combination after organic contamination. Photoelectron signals related to organic contaminants are mainly detected at a binding energy of approximately 285 eV.[35,36] Thus, significant organic contamination remains on the surface in the case of annealing only in vacuum. However, the amounts of organic contaminants are reduced for the sample annealed in air and vacuum combination. Therefore, annealing only in vacuum cannot be an alternate process to annealing in air. We propose that the best performance of plasma discharge devices with (Mg,Ca)O protective layers can be realized by the addition of annealing in vacuum before the panel sealing process.

4. Conclusions

The quantitative relationships between V_{sus} and carbonation ratio, and the decarbonation annealing of carbonated (Mg,Ca)O protective layers in plasma discharge devices were investigated. A high V_{sus} was obtained and a low V_{sus} was also realized, as expected. This degradation of V_{sus} was quantitatively assigned to the carbonation of Ca. To suppress Ca carbonation, dry air is a more suitable atmosphere than humid air for exposure. The carbonation of Ca cannot be reversed by annealing in the air atmosphere at an accessible temperature; therefore, annealing in vacuum is proposed for the decarbonation of (Mg,Ca)O protective layers, which resulted in the lowering of V_{sus}. The additional process of annealing in vacuum after annealing in air should be performed immediately before panel sealing for the production with (Mg,Ca)O protective layers to satisfy both the removal of organic residues on the protective layer during production and the decarbonation of (Mg,Ca)O films. The proposed process will lead to practical applications of high-γ materials as a protective layer used for not only plasma displays but also other plasma discharge devices containing high Xe contents with high luminous efficiencies and low discharge voltages.

Acknowledgments

This work was mainly carried out by the PDP Advanced Development Group, PDP Devices Business Unit, Visual Products and Display Devices Business Group, AVC Networks Com-

pany, Panasonic Corporation. This work was partially supported by the Image Devices Development Center, Corporate R&D Division, and the Production Engineering Laboratory, Manufacturing Technology and Engineering Division of Panasonic Corporation.

References

1) U. Kogelschatz, Plasma Chem. Plasma Process. **23**, 1 (2003).
2) H. Uchiike and T. Hirakawa, Proc. IEEE **90**, 533 (2002).
3) J. P. Boeuf, J. Phys. D **36**, R53 (2003).
4) L. F. Weber, IEEE Trans. Plasma Sci. **34**, 268 (2006).
5) M. Ilmer, R. Lecheler, H. Schweizer, and M. Seibold, SID Symp. Dig. Tech. Pap. **31**, 931 (2000).
6) T. Shiga, Y. Ikeda, S. Mikoshiba, and S. Shinada, J. Light Vis. Environ. **25**, 10 (2001).
7) Y. Aoyagi and N. Kurose, Appl. Phys. Lett. **102**, 041114 (2013).
8) T. Zukawa, Y. Sasaki, H. Tsujimoto, N. Kamiko, and E. Nakamura, Proc. Int. Ultraviolet Assoc. World Congr., 2016.
9) H. Uchiike, K. Miura, N. Nakayama, T. Shinoda, and Y. Fukushima, IEEE Trans. Electron Devices **23**, 1211 (1976).
10) J. Meunier, Ph. Belenguer, and J. P. Boeuf, J. Appl. Phys. **78**, 731 (1995).
11) G. Oversluizen, T. Dekker, M. F. Gillies, and S. T. de Zwart, SID Symp. Dig. Tech. Pap. **34**, 28 (2003).
12) Z. Liu, W.-B. Hu, and C.-L. Liu, IEEE Trans. Plasma Sci. **38**, 2860 (2010).
13) H. Uchiike, K. Sakiya, T. Hashimoto, T. Shinoda, and Y. Fukushima, IEEE Trans. Electron Devices **30**, 1735 (1983).
14) Y. Motoyama, Y. Murakami, M. Seki, T. Kurauchi, and N. Kikuchi, IEEE Trans. Electron Devices **54**, 1308 (2007).
15) G. Uchida, F. Xing, S. Uchida, T. Yano, N. Awaji, H. Kajiyama, and T. Shinoda, Proc. 15th Int. Disp. Workshops, 2008, Vol. 2, p. 781.
16) G. Pacchioni, J. M. Ricart, and F. Illas, J. Am. Chem. Soc. **116**, 10152 (1994).
17) M. B. Jensen, L. G. M. Pettersson, O. Swang, and U. Olsbye, J. Phys. Chem. B **109**, 16774 (2005).
18) T. Shinoda, H. Uchiike, and S. Andoh, IEEE Trans. Electron Devices **26**, 1163 (1979).
19) T. J. Vink, A. R. Balkenende, R. G. F. A. Verbeek, H. A. M. van Hal, and S. T. de Zwart, Appl. Phys. Lett. **80**, 2216 (2002).
20) Y. Fukui, Y. Honda, Y. Yamauchi, M. Okafuji, M. Sakai, M. Nishitani, and Y. Takata, J. Soc. Inf. Disp. **18**, 1090 (2010).
21) Y. Yamauchi, Y. Fukui, Y. Honda, M. Okafuji, M. Sakai, M. Nishitani, and Y. Yamauchi, IEICE Trans. Electron. **E95-C**, 1761 (2012).

22) T. Yano, G. Uchida, K. Uchida, N. Awaji, T. Shinoda, and H. Kajiyama, Proc. 16th Int. Disp. Workshops, 2008, Vol. 3, p. 1933.
23) M. Hasegawa, S. Fukui, and K. Betsui, Proc. 16th Int. Disp. Workshops, 2009, Vol. 3, p. 1941.
24) K.-W. Whang, T.-H. Lee, and H.-W. Cheong, SID Symp. Dig. Tech. Pap. **41**, 732 (2010).
25) J. Cho, R. Kim, K.-W. Lee, G.-Y. Yeom, J.-Y. Kim, and J.-W. Park, Thin Solid Films **350**, 173 (1999).
26) Y. Motoyama, D. Kato, and M. Seki, Proc. 17th Int. Disp. Workshops, 2010, Vol. 2, p. 959.
27) Q. Yan, X. Deng, Z. Lu, F. Xing, X. Zhang, C. Tang, and H. Wei, SID Symp. Dig. Tech. Pap. **42**, 633 (2011).
28) T. Zukawa, K. Yoshino, Y. Oe, H. Kawarazaki, K. Aoto, Y. Tanaka, and R. Murai, SID Symp. Dig. Tech. Pap. **43**, 165 (2012).
29) T.-H. Lee, H.-W. Cheong, O. Kwon, and K.-W. Whang, IEEE Trans. Electron Devices, **60**, 301 (2013).
30) S. Jeong, J.-S. Kim, and Y.-S. Kim, SID Symp. Dig. Tech. Pap. **44**, 131 (2013).
31) M. Amatsuchi, A. Hirota, H. Lin, T. Naoi, E. Otani, H. Taniguchi, and K. Amemiya, Proc. 12th Int. Disp. Workshops, 2005, Vol. 1, p. 435.
32) P. E. Larson and M. A. Kelly, J. Vac. Sci. Technol. A **16**, 3483 (1998).
33) D. A. Shirley, Phys. Rev. B **5**, 4709 (1972).
34) P. Swift, Surf. Interface Anal. **4**, 47 (1982).
35) S. L. Stipp and M. F. Hochella, Jr., Geochim. Cosmochim. Acta **55**, 1723 (1991).
36) F. Khairallah and A. Glisenti, Surf. Sci. Spectra **13**, 58 (2006).
37) J. C. Fuggle, L. M. Watson, D. J. Fabian, and S. Affrossman, J. Phys. F **5**, 375 (1975).
38) R. Nowosielski, A. Bajorek, and R. Babilas, J. Non-Cryst. Solids **447**, 126 (2016).
39) M. Engelhard and D. Baer, Surf. Sci. Spectra **6**, 153 (1999).
40) D. Ochs, M. Brause, B. Braun, W. Maus-Friedrichs, and V. Kempter, Surf. Sci. **397**, 101 (1998).
41) D. Ochs, B. Braun, W. Maus-Friedrichs, and V. Kempter, Surf. Sci. **417**, 406 (1998).
42) Y. Motoyama, D. Kato, N. Saito, and M. Seki, J. Soc. Inf. Disp. **21**, 41 (2013).
43) H. D. Hagstrum, Phys. Rev. **122**, 83 (1961).
44) M. O. Aboelfotoh and J. A. Lorenzen, J. Appl. Phys. **48**, 4754 (1977).
45) M. Sakai, S. Hatta, Y. Fukui, Y. Honda, M. Okafuji, Y. Yamauchi, M. Nishitani, and Y.

Tanaka, Proc. 15th Int. Disp. Workshops, 2008, Vol. 3, p. 1881.

46) S. Ardizzone, C. L. Bianchi, M. Fadoni, and B. Vercelli, Appl. Surf. Sci. **119**, 253 (1997).

47) V. Manovic and E. Anthony, Environ. Sci. Technol. **41**, 1420 (2007).

48) T. Nakayama, M. Terauchi, K. Yoshino, T. Tsujita, M. Nishitani, T. Ishituka, T. Tomie, and Y. Morita, Proc. 17th Int. Disp. Workshops, 2010, Vol. 3, p. 1963.

49) K. Yoshino, Y. Morita, T. Nagatomi, M. Terauchi, T. Tsujita, Y. Doi, T. Nakayama, Y. Yamauchi, M. Nishitani, M. Kitagawa, Y. Takai, and Y. Yamauchi, SID Symp. Dig. Tech. Pap. **42**, 641 (2011).

50) K. Yoshino, Y. Morita, T. Nagatomi, M. Terauchi, T. Tsujita, Y. Doi, T. Nakayama, Y. Yamauchi, M. Nishitani, M. Kitagawa, Y. Yamauchi, and Y. Takai, Appl. Surf. Sci. **259**, 135 (2012).

51) K. H. Stern and E. L. Weise, *High Temperature Properties and Decomposition of Inorganic Salts*. *Part 2*. *Carbonates* (U.S. Government Printing Office, Washington, D.C., 1969) Chap. B.